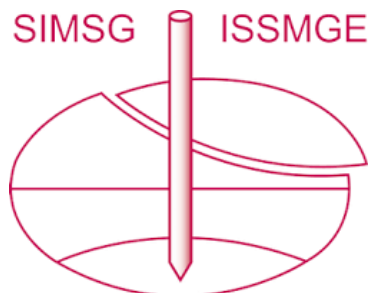


INTERNATIONAL SOCIETY FOR SOIL MECHANICS AND GEOTECHNICAL ENGINEERING



This paper was downloaded from the Online Library of the International Society for Soil Mechanics and Geotechnical Engineering (ISSMGE). The library is available here:

<https://www.issmge.org/publications/online-library>

This is an open-access database that archives thousands of papers published under the Auspices of the ISSMGE and maintained by the Innovation and Development Committee of ISSMGE.

How do fabric and dilatancy affect the strength of granular materials

De la manière dont la microstructure et la dilatance influent la résistance des matériaux granulaires

R.G. Wan, M. Al-Mamun

Department of Civil Engineering, University of Calgary, Alberta, Canada

P.J. Guo*

Department of Civil Engineering, McMaster University, Ontario, Canada

ABSTRACT: The paper explores the role of dilatancy on the shear strength of a granular material by highlighting both of its particulate nature and microstructure. A fabric embedded stress dilatancy equation is used in an elastoplastic model to demonstrate fabric-dilatancy related sand behaviour. The importance of dilatancy is highlighted by examining sand response along loading paths other than drained and undrained conditions. It is found that the strength of sand is not at all bounded by the ones obtained in drained and undrained conditions. It turns out that lower strengths are encountered under strain paths with forced dilation or compaction. This is confirmed by microstructural observations made on a granular assembly of photoelastic particles loaded biaxially.

RÉSUMÉ: Cette communication cherche à démontrer le rôle de la dilatance sur la résistance d'un matériau granulaire selon sa nature microstructurelle. On utilise une relation de dilatance incorporant l'aspect microstructurelle dans un modèle élastoplastique pour illustrer l'aspect dilatance-microstructure du comportement d'un sable. En particulier, on étudie la réponse d'un sable selon un chemin de déformation autre que le cas non-drainé ou drainé. La résistance d'un sable n'est pas bornée par les valeurs obtenues en condition drainée ou non-drainée. Il se peut que le sable ait une résistance plus faible selon d'autres chemins dilatants ou contractants. Ces conclusions convergent avec des résultats d'expérience sur un matériau granulaire 2-D, formé de disques photoélastiques.

1 INTRODUCTION

In geotechnical practice, the strength of sand is solely described by an ubiquitously used friction angle φ . However, it is surprising to note how little attention is actually paid to the dilatancy angle, and even worse, to the fabric or microstructural aspects of the material. It is important to discriminate between the various friction angles known in soil mechanics, namely peak friction and constant volume (critical state) friction angles in relation to the dilatancy angle, pressure, density, and fabric levels. The dilatancy angle, defined at the macroscopic scale, emanates directly from the very fact that sand is a particulate material and grain over-riding to produce an increase in volume is inevitable. The microstructure (fabric) of the sand acts as an internal kinematic constraint against applied stresses, giving rise to volume dilation with a concomitant apparent increase in strength. Therefore, it is important to embed fabric during material characterization, given that it governs its propensity to dilate, and hence its strength. For instance, it is well known that the shear strength as determined from conventional triaxial tests is very much dependent on the method of sample preparation, namely wet tamping and air pluviation, see among others Zlatovic and Ishihara (1997). If a metric was adopted for describing fabric by way of a so-called fabric tensor and incorporated into the interpretation of experimental results, then we would arrive at a more objective measure of material strength. This argument is especially pertinent to natural soils with microstructure that succumb to instability in the form of strain localization and liquefaction.

The above issues motivate the present paper, whose primary goal is to describe the stress-dilatancy of granular soils in terms of fabric, density and pressure levels as an extension to Rowe's (1962) theory, and thereafter demonstrate departures from 'normal' behaviours of sand under various fabric and loading conditions. The second goal of this communication is to offer fabric related experimental support to model simulations presented in the first part of the paper.

As a prelude we recall various experimental observations that highlight the roles of dilatancy and fabric on the shear strength of a granular material.

2 EXPERIMENTAL OBSERVATIONS

There are numerous examples of fabric dependence and dilatancy behaviour of granular materials in monotonic loading. Fig. 1 shows the stress/strain/volumetric strain responses of a sand specimen tested in drained triaxial compression (Oda, 1972). The specimen was reconstituted by pluviating sand at different initial bedding planes while maintaining sensibly the same void ratio in each case. It is clear that the specimen with a horizontal bedding plane ($\theta = 0^\circ$) gives a higher deviatoric stress (shear strength) than the one with vertical bedding planes ($\theta = 90^\circ$). It also follows that the specimen with horizontal bedding planes dilates more as confirmed in Fig. 1b. As such, the shear strength of a non-cohesive frictional material exhibits a strong dependence on particulate microstructure, hence fabric and dilatancy.

Because of the intrinsic effect and importance of fabric, the bearing capacity of a shallow footing on a dense sand deposit with inherent structure by way of bedding planes will exhibit variations in bearing capacity just like the specimens discussed in the previous example. Fig. 2 essentially illustrates the effect of strength anisotropy on the bearing capacity of a foundation soil (Oda and Koishikawa, 1979).

The intertwined roles of dilatancy and fabric are perhaps most evident in the case of drained cyclic loading of sand involving principal stress direction reversals. This is typified in a soil-structure interaction problem that involves slow movements of a retaining wall at small amplitudes in such a way that the granular backfill is set into alternating active and passive pressures.

Fig. 3 shows the deformation pattern associated with such a loading as observed in a sand box experiment recently performed by the authors. The main characteristic of the deforma-

* second author

tion in the sand is retrogressive failure with multiple shear banding and progressive densification of the failure wedge to ultimately activate a passive failure surface far back behind the wall. The underlying mechanism is one in which, volume changes together with fabric evolve cycle by cycle and control both the stiffness and stability of the granular soil. The analogue of the problem is a sand specimen being subjected to drained cyclic loading (Nakata et al. 1992). Fig. 4 shows the evolution of dilatancy cycle by cycle with a progressive densification and decrease of the threshold stress ratio defining phase change, i.e. the transition from contractancy and dilatancy.

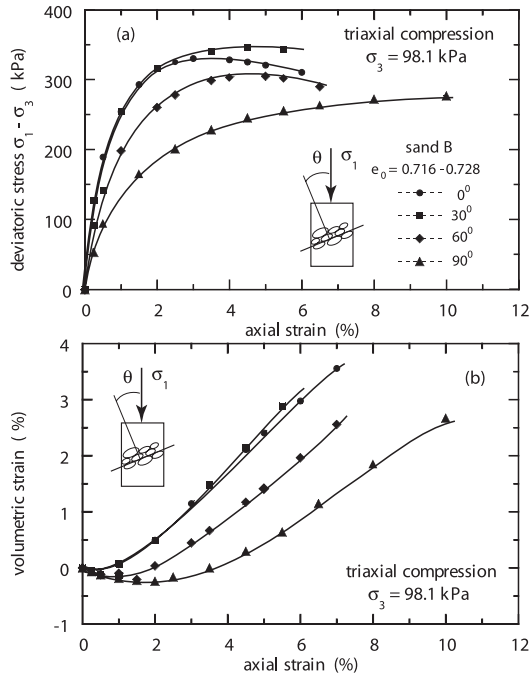


Figure 1. Response of reconstituted sand as a function of initial bedding plane: (a) deviatoric stress and (b) dilatancy – after Oda (1972)

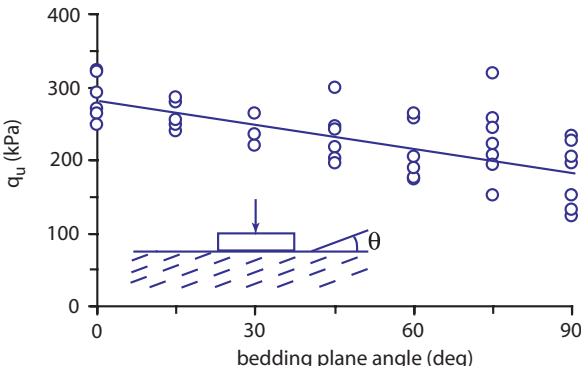


Figure 2. Effect of strength anisotropy on bearing capacity – after Oda and Koishikawa (1979)

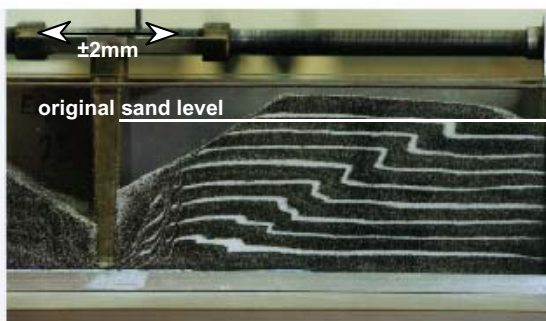


Figure 3. Failure mechanism in sand subjected to slow cyclic loading

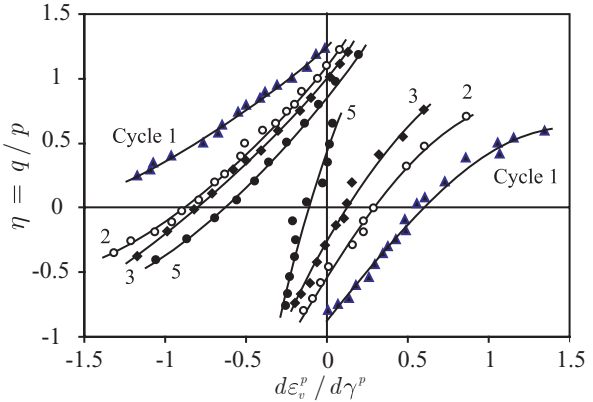


Figure 4. Evolution of dilatancy in drained cyclic loading of a sand specimen – after Nakata et al. (1992)

3 STRESS DILATANCY THEORY

The phenomenon of dilatancy was first revealed by Reynolds (1885) and has fascinated researchers over centuries with pioneering works from Caquot (1934), Taylor (1948), Newland and Alley (1957), to name a few. In geotechnical engineering, the dilatancy behaviour of soils is usually described within Rowe's (1962) stress-dilatancy theory for its practicality. By minimizing the ratio of the rate of work done on an assembly of particles by the major principal stress to the rate of work done by the minor principal stress, Rowe arrived at his celebrated dilatancy equation, i.e.

$$\frac{\sigma_1}{\sigma_3} = KD; K = \tan^2(45^\circ + \varphi_\mu); D = 1 - \frac{\dot{\epsilon}_v^p}{\dot{\epsilon}_1^p} \quad (1)$$

where φ_μ = interparticle friction angle, $\dot{\epsilon}_v^p$ = plastic volumetric strain rate, $\dot{\epsilon}_1^p$ = axial plastic strain rate, while σ_1 and σ_3 are applied major and minor principal stresses respectively. Eq. (1) indicates that the dilatancy term D is a function of the applied stress ratio and the interparticle friction. Referring back to the experimental observations described in the previous section, it is clear that dilatancy is a function of fabric (Fig. 1) and density of packing (Fig. 4). These dependencies vitiate the predictive capability of Rowe's stress dilatancy model (Eq. 1). There have been since many works on stress dilatancy towards addressing the above-mentioned shortcomings, among many others, it is worth mentioning the works of Wan and Guo (1998) and Li and Dafalias (2000) towards incorporating the effect of void ratio and stress level.

As for dealing with fabric changes during the dilatant phase of sand deformation, Dafalias and Manzari (2004) used a bounding surface plasticity framework with the plastic modulus degrading with fabric. Other approaches which are still macroscopic in nature focus at capturing detailed particle mechanics such as the double sliding model worked out by Balandran and Nemat-Nasser (1993). Since fabric operates directly on the way dilatancy is manifested, it is worthwhile summarizing briefly at the outset the underlying concepts of the fabric embedded stress dilatancy model developed by Wan and Guo (2001a, 2004). This model will be used in the paper to illustrate the capability of constitutive models to capture some of the micromechanical behavioural features of sand.

3.1 Fabric embedded stress-dilatancy model

In view of incorporating microstructural aspects into the formulation of stress-dilatancy, a representative elementary volume (REV) is chosen in which micro-variables are averaged and expressed in terms of macro-variables. For example, as a result of

volume averaging, contact forces between particles can be expressed in terms of Cauchy stress, σ , via a so-called fabric tensor, F , that describes the geometrical arrangement of particles. Similarly, global strains ϵ can be linked to fabric and kinematical variables such as particle translations and rotations. Details can be found in Guo (2000) and Chang & Ma (1991).

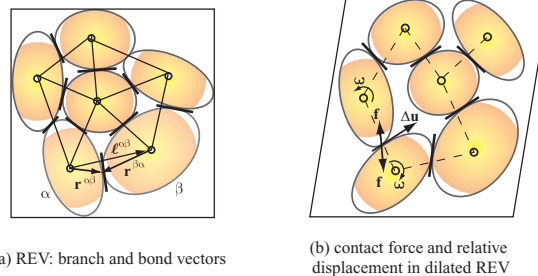


Figure 5. Granular assembly in REV and graph representation of contact topology

Fig. 5a. shows a cluster of rigid particles chosen in a REV with particle connectivity represented by a graph of branch vectors ℓ and bond vectors r . During the deformation of the REV, particles slide and rotate as shown in Fig. 5b giving rise to macroscopic volume change of the REV with an associated change in the graph structure of particle connectivity, hence fabric. Fabric can be essentially represented by a second order tensor formed of the dyadic product of local branch vectors such as

$$F_{ij} = \frac{1}{V} \sum_{\text{contacts}} \ell_i^c \ell_j^c dV \quad (2)$$

The essence of the proposed dilatancy model is to write energy dissipation considerations at grain contacts that slip and rotate during macroscopic deformations. For energy conservation at both scales, the rate of energy (power) dissipated \dot{D} at the microscopic level must be equal to the work rate \dot{W} expressed in terms of macro-variables, i.e.

$$\dot{W} = \sigma : \dot{\epsilon} = \frac{1}{V} \int_{\text{sliding}} \dot{D}(\epsilon) dV \quad (3)$$

over sliding contacts. The power dissipated \dot{D} can be further expressed in terms of micro-variables such as average tangential contact forces and relative slip displacements. As a result of such principle, a stress dilatancy equation with embedded micro-variables emerges in the form of a dilatancy rate defined as the ratio of volumetric strain rate, $\dot{\epsilon}_v$, over shear strain rate, $\dot{\gamma}$. These strain rates are wholly plastic. In conventional triaxial (axial symmetry) stress states, we get

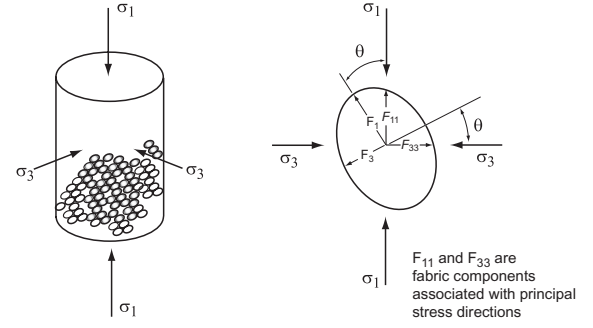
$$\sin \psi = \frac{\dot{\epsilon}_v}{\dot{\gamma}} = \frac{4}{3} \frac{(\sin \varphi_m - \sin \varphi_f)}{(1 - \sin \varphi_f \sin \varphi_m)} \quad (4)$$

in which ψ = dilatancy angle, φ_m = mobilized friction angle, and φ_f = characteristic friction angle. For details, see Wan and Guo (2001a, b). It is interesting to note that Eq. (4) takes essentially the same form as the standard Rowe's dilatancy equation (if Eq. 1 is recast in terms of mobilized friction angle using Mohr-Coulomb criterion), except for a characteristic friction angle herein introduced to establish the link to fabric, i.e.

$$\sin \varphi_f = \frac{X(F_{33}/F_{11}) + \bar{\gamma}}{a + \bar{\gamma}} \left(\frac{e}{e_{cr}} \right)^\alpha \sin \varphi_{cv} \quad (5)$$

where e and e_{cr} are current and critical void ratios respectively, φ_{cv} is the friction angle at critical state, while X , α and a are constants. Fabric information is transmitted through fabric components F_{11} and F_{33} which are projections of the second order fabric tensor F_{ij} (Wan & Guo, 2001a) along principal stress directions σ_1 and σ_3 respectively, and $\bar{\gamma}$ the transformed plastic shear strain term which factors conventional

strain to fabric. In general, fabric and stress tensors are not coaxial. Fig. 6 illustrates the fabric tensor and its components relative to the principal stress directions.



(a) sand specimen in axial symmetry subjected to principal stresses
(b) orientation θ of the major principal axis of fabric tensor F with principal stress direction
Figure 6. Representation of fabric tensor and its components with respect to principal stress directions.

Turning back to Eq. (4), it is evident that both positive and negative rates of dilation can be obtained depending on the relative magnitude of φ_m to φ_f . In the limit, fabric conditions can be such that a positive rate of dilation is possible even though the current void ratio is looser of critical, i.e. $e > e_{cr}$. By the same token, for a small mobilized friction angle (hence stress ratio), Eq. (4) can capture dilation. Hence, the proper evolution of dilatancy as observed during drained cyclic loading as illustrated in Fig. 4 can be contemplated. A modified form of Eq. (4) to accommodate for cyclic loading has been worked out by Wan and Guo (2001b).

4 DILATANCY, FABRIC AND STRENGTH ISSUES IN PROPORTIONAL STRAIN LOADING

In the following discussions, our attention will be restricted to a class of granular material response that results from the imposition of a constant dilation rate parameterized by the ratio of imposed volumetric to shear strains, i.e. $\vartheta = \dot{\epsilon}_v / \dot{\gamma}$, on the material. Therefore, a value of $\vartheta=0$ corresponds to isochoric (undrained) deformations, while constant compaction and dilation rate tests refer to positive and negative ϑ values respectively. These tests, essentially proportional strain path tests, were conducted by Chu et al. (1992) to probe strain-softening and localization of sand. From a practical viewpoint, Vaid and Sivathayalan (2000) have also investigated strain path tests by controlling the drainage conditions in the test specimen since water flowing into or out of it would cause either dilation or contraction. The rationale of such tests is that under real field situations, soils deform in a partially drained condition which is thought to be conducive to fabric changes.

4.1 Modelling proportional strain paths via stress-dilatancy

In the next discussions, numerical simulations of sand behaviour will be conducted using an elastoplastic model with the fabric embedded stress-dilatancy Eq. (4) as a flow rule. Fig. 7 shows the predictions obtained for medium dense ($e_0=0.6$) Ottawa sand tested along a variety of proportional strain paths covering the whole range of possible dilation and compaction rates ($\vartheta=-0.8$ to $+1.08$) at a confining pressure of 200 kPa. The response of sand changes from a stable (hardening) behaviour for strain paths that are mostly compactive, to one which is dominantly unstable (strain-softening) for dilatant paths. It is also observed that the behaviour of the sand is not at all bounded by the drained and isochoric (undrained) responses.

Therefore, it would be somewhat erroneous to determine the strength of a sand solely based on drained or undrained conditions. There are, in fact, worst conditions under which the soil could succumb to instability, and thereby display marginal strength. Also, the maximum deviatoric stresses corresponding to the unstable responses ($\vartheta = -0.4$ & -0.8) are well below the Critical State Line (CSL).

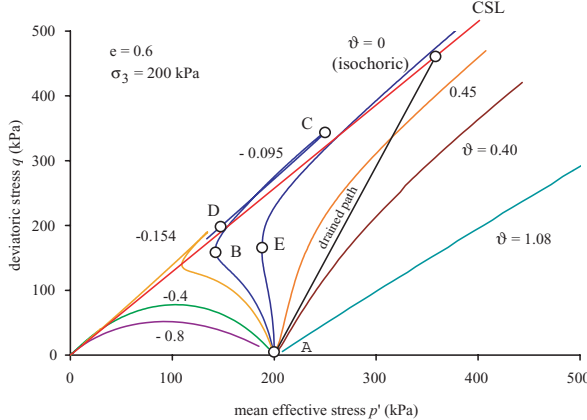


Figure 7. Stress response paths for sand subjected to various proportional strain paths

For strain paths corresponding to moderate dilation rates, say $\vartheta = -0.095$, it is seen that the sand initially displays a hardening behaviour (path ABC) until a stress level at which stability cannot be any longer sustained and collapse occurs (path CD). This ‘snap-back’ phenomenon has been in fact observed experimentally by Chu et al. (1992) and can be explained via dilatancy and microstructural arguments. Fig. 8 shows the evolution of mobilized material background dilatancy with deviatoric stress referring to the stress paths in Fig. 7.

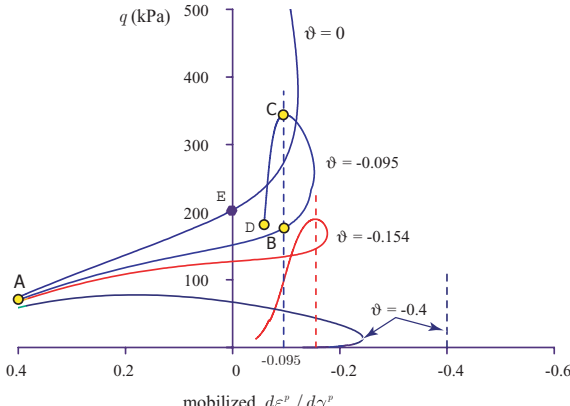


Figure 8. Mobilized dilatancy as a function of deviatoric stress

We are particularly interested in the path ABCD that corresponds to an overall volume dilation of the specimen with deformation rate $\vartheta = -0.095$. Initially, at small mobilized friction angles, the material exhibits compressive volumetric strains following its stress-dilatancy characteristics as a background response. In order to satisfy the volumetric constraint imposed on the specimen, the mean effective stress should decrease with an increase in deviatoric stress in order to meet with the imposed dilation (path AB in Figs. 7 and 8). As deformation proceeds, the mobilization of friction angle becomes more prominent so that the material background behaviour is dilative according to the stress-dilatancy equation. This may lead to an increase in dilatancy that may exceed the imposed rate of volume expansion. In order to satisfy the imposed volumetric constraint, both the effective mean and deviatoric stresses now have to increase (path BC) to compensate for the extra dilation. As the mean effective stress increases, the dilatancy rate decreases, and a point

C is reached at which the dilatancy rate is the same as the imposed rate of volume change again. When point C is passed, however, the mobilized dilatancy is smaller than the imposed rate of volume expansion. Consequently, the mean effective stress must decrease to satisfy the constraint of the imposed rate of volume change, as shown by path CD. If the maximum mobilized dilatancy rate is less than the imposed rate of volume expansion, the mean effective stress decreases monotonically, as for the case of $\vartheta = -0.4$. On the other hand, for an undrained test with $\vartheta = 0$, when the effective stress path passes the phase transformation state (point E), the sand sample continues dilating and the deviatoric stress q monotonically increases until the ultimate deformation state is reached.

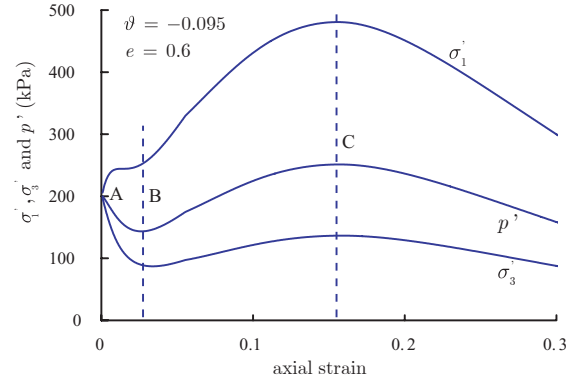


Figure 9. Evolution of effective stress components

Finally, Fig. 9 shows the variation of effective stress components along the imposed strain path $\vartheta = -0.095$. Along AB, the effective axial stress σ_1' increases while the lateral stress σ_3' decreases, giving a net decline in mean effective stress. On path BC, the increase in both σ_1' and σ_3' results in a net increase in mean effective stress until a maximum is reached at point C where the snap back takes place. All stresses decrease after point C as the material collapses.

It transpires from the discussions of this section that generally speaking, a granular material has a certain potential to dilate preset by its fabric. It is the nature of the loading conditions imposed on the material that will allow it to express a certain amount of dilatancy. The amount of dilation that is ‘unlocked’ is representative of the material shear strength.

4.2 Biaxial loading of photoelastic grains along proportional strain paths

On the best ways to study microstructural changes during deformation history is to resort to an analogue granular material consisting of photoelastic grains and optically observe the force transmission by means of fringes developed at contact points. In the following, we examine the biaxial loading of an ensemble of photoelastic disks, and observe the particle force chains developed at different deformation states. In fact, various rates of dilation are imposed on the ensemble (specimen) with predetermined axial and lateral displacement rates (\dot{D}_1 & \dot{D}_2) in a ratio $\vartheta^* = (\dot{D}_1 + \dot{D}_2) / (\dot{D}_1 - \dot{D}_2)$. The material response is expressed in terms of axial and lateral forces F_1 and F_2 respectively. The analogue of these tests in axi-symmetric stress and strain conditions was discussed in the preceding section.

Fig. 10 shows the force response paths plotted as deviatoric force ($F_d = F_1 - F_2$) against mean force ($F_m = F_1 + F_2$) for selected imposed rates of dilation, i.e. ϑ^* values. The force response paths of 2-D granular materials biaxially loaded bear a striking resemblance to the stress response paths of sand tested in axisymmetric stress and strain conditions. For comparison purposes, we note for the former case the ‘coarseness’ of the granular assembly which comprised of roughly 300 pentagonal

shaped photoelastic particles packed in a random isotropic fashion prior to shearing.

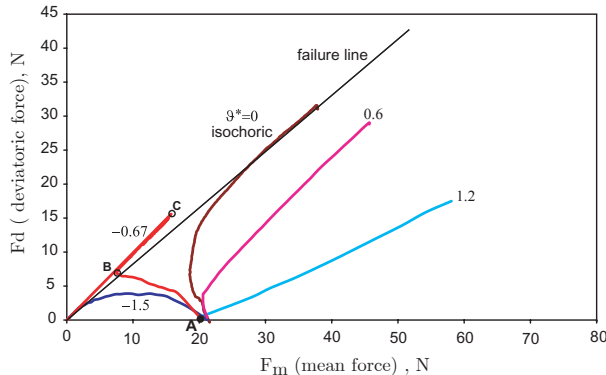


Figure 10. Force responses of the photoelastic disk assembly

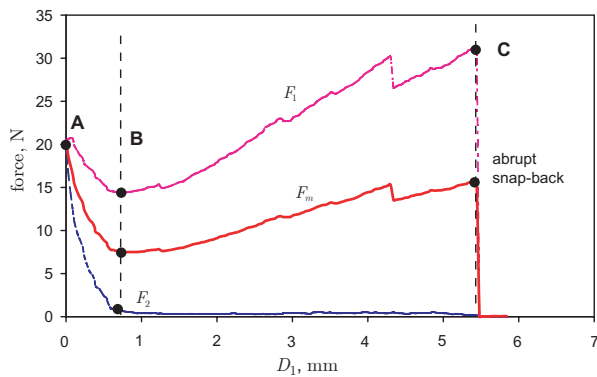


Figure 11. Force component evolution along path ABC

The evolution of axial and lateral forces F_1 and F_2 is shown in Fig. 11 for the path $\vartheta^* = -0.67$ in particular. In general, we observe a quite similar trend as the one described in Fig. 9 for model simulations, in which forces/stresses drop (A-B) and then rise (B-C).

Finally, Fig. 12 reveals the contact force chain and associated structure at key points A, B and C on the force response curve plotted in Fig. 10. The fringe patterns indeed indicate the formation of contact force chains as we move from A to B on the force response path with a reduction in both axial and lateral loads. Between B and C, additional force chains develop in the axial direction so that the axial load picks up. At the same time, in order to sustain the deformation as prescribed by ϑ^* , the lat-

eral load has to decrease so as to allow for the required dilation. The force chains ultimately buckle at point C corresponding to the snap back. It is also interesting to note that a two-phase structure emerges with the force chains seen embedded into a matrix of apparently less loaded particles. The mechanism of contact force chain build up and buckling concur with the model simulations presented in the previous section. This suggests that it is possible to describe micro/meso phenomena through a continuum level model with an embedded fabric tensor.

Superimposed on the ‘photoelastic’ images in Fig. 12 are the polar plots of void ratio distributions conveying their directional nature as a function of loading history along path ABC. The directional void ratio plots were created by drawing a series of scan lines radiating from the centre of the specimen. Each radial line intersects a number of grains as well as voids along its run. The lineal void ratio along a scan line is simply defined as the ratio of the length of intersected voids to that of solid. The raw data has also been smoothed out using a high order Fourier series as shown by the continuous void ratio distribution. Initially, at point A, the packing is almost isotropic with an average lineal void ratio of 0.2 approximately. At the turning point (pt. B), the formation of force columns in the axial direction is reflected by a generalized reduction in void ratio in that same direction, while void ratio increases in other directions. At the point of collapse (C), the buckling of the columns produce loosening of the packing in the lateral direction as confirmed by the rotation of the void ratio distribution.

Next, it is worthwhile to establish the contribution of dilatancy to shear strength as deduced from some apparent friction angle φ_p deduced from the asymptotic part of force response paths given in Fig. 10. If α is the angle of inclination of the asymptotic part of the force response path in the F_m versus F_d axes, and invoking a Mohr-Coulomb failure criterion, it turns out that $\sin \varphi_p = \tan \alpha$. In addition, recalling the imposed dilation rate as $\vartheta^* = (\dot{D}_1 + \dot{D}_2) / (\dot{D}_1 - \dot{D}_2)$, we can obtain a dilatancy angle ψ based on kinematical conditions, and considering the Mohr’s circle of strains (Hansen, 1958), it follows that

$$\sin \psi = (\dot{D}_1 + \dot{D}_2) / (\dot{D}_1 - \dot{D}_2) = \vartheta^* \quad (6)$$

Since for each test, the enforced dilation rate ϑ^* (hence dilatancy angle ψ) is known, a relationship between the apparent friction angle, φ_p , as derived from α and dilation angle can be established. Table 1 shows the measured as well as transformed data from a more complete set of tests than the ones given in Fig. 10.

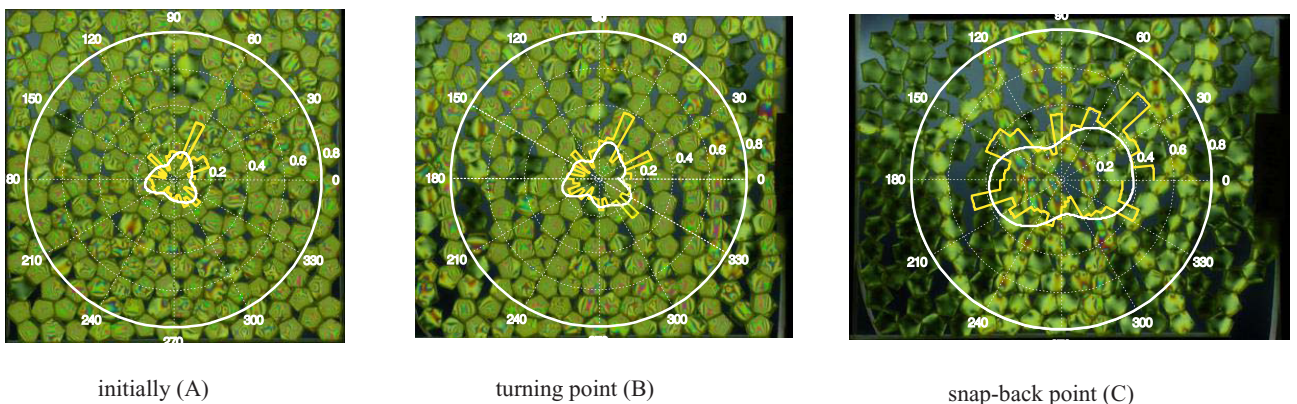


Figure 12. Fabric evolution along dilatant strain path ABC: consolidation of grains, formation of strong force columns, and spontaneous buckling of force chains due to loss of lateral confinement. Also, the evolution of the directional void ratio plot confirms the mechanism of deformation.

Table 1: Dilation angles observed from static and kinematic analyses

θ^*	α (deg)	φ_p (deg)	$\varphi_p - \varphi_{cv}$	$\sin^{-1}(\theta^*)$
0	39.8	56.4 (= φ_{cv})	0	0
-0.2	41.5	62.1	5.7	11.5
-0.33	42.1	64.5	8.1	19.3
-0.60	43.18	69.8	13.4	36.8
-0.67	44	74.9	18.5	42
-0.75	45	90	33.6	48.6

From the above data, we arrive at the following simple relationship, i.e.

$$\varphi_p = \varphi_{cv} + 0.4\psi \quad (7)$$

We note that the above relationship established is similar to the one developed by Bolton (1986), i.e.

$$\varphi_p = \varphi_{cv} + 0.8\psi \quad (8)$$

which was derived from experimental data on sand.

5 SUMMARY AND CONCLUSIONS

The strength of a granular material is inextricably related to its dilatancy or contractancy, a mere reflection of its initial fabric and evolution. Fabric changes are bound to occur when strains rather than stresses are imposed to a volume of material. Hence, in proportional strain paths tests, it is found that a medium dense sand can display an unstable behaviour for particular imposed dilation rates, while it is very well stable over contraction rates. Clearly, the strength of soils is a function of the dilation rate applied to it, and is not bounded by the undrained (zero volumetric strain rate) and drained cases. Thus, using the drained and undrained shear strengths values in practice to bracket the actual strength of soil may be erroneous. In fact, the strength of a soil is a function of loading conditions imposed on it. A good example is the case illustrated in this paper in which slow cyclic rotation of a retaining wall imparts both fluctuating strains and rotation of principal stress directions to the granular backfill. Another case refers to partial drainage conditions in the field, whereby there is local influx or efflux of water enforcing imposed dilation or contraction to a soil element. It is also worth mentioning the phenomenon of gas ex-solution in gassy soils in which the rate of production of gas makes the soil skeleton compressible. As a result, the soil skeleton deforms according to the rate of gas production, and as such, the soil element is subjected to strain paths with dilatancy/contractancy rates akin to the ones discussed in this paper.

It was also shown in the paper that limiting stresses such that they stay within a failure envelope (surface) is not sufficient to prevent failure of granular materials. There may be stress states within such a surface, under some particular loading conditions like those with imposed dilation rates, whereby the material displays an unstable (softening) behaviour deforming with unlimited strains in a flow fashion. This behaviour is very well dictated by both microstructure and dilatancy of the material as revealed in the biaxial shearing of an assembly of photoelastic disks. The mechanism by which materials derive their strength is reflected in the way stresses/forces are carried by the microstructure. A spontaneous flow type of behaviour with softening is in fact due to the local buckling of force chains at the micro level. The granular material consists of a two ‘phase’ material composed of a strong network of forces supported by a weaker one. It is the disruption of the delicate balance between the two networks that governs the material stability, hence strength of a granular material.

As a final note, we emphasize that the deformation behaviour of granular soils is indeed complex and controlled by

their fabric and propensity to dilate. It is not sufficient to test geomaterials in solely drained and undrained conditions. Other loading conditions and controlling parameters must be sought for which the material strength may soften and become unstable.

ACKNOWLEDGEMENT

The authors wish to acknowledge funding provided by the Natural Science and Engineering Research Council of Canada.

REFERENCES

- Balandran, N., and Nemat-Nasser, S. 1993. Double sliding model for cyclic deformation of granular materials, including dilatancy effects. *J. Mech. Phys. Solids*, 41(3), 573-612.
- Bolton, M.D. 1986. The strength and dilatancy of sands. *Geotechnique*, 35(2), 99-112.
- Caquot, A. 1934. *Equilibre des massifs à frottement interne: Stabilité des terres pulvérulentes et cohérentes*. Gauthier Villars, Paris.
- Chang, C.S. and Ma, L. 1991. A micromechanical-based micropolar theory for deformation of granular solids. *Int. J. Solids Structures*, 28(1), 67-86.
- Chu, J., Lo, S-C.R. and Lee, I.K. 1992. Strain-softening behaviour of granular soil in strain-path testing. *J. Geotech. Eng. ASCE*, 118(2), 191-208.
- Dafalias, Y. and Manzari, M. T. 2004. Simple plasticity sand model accounting for fabric change effects. *J. of Eng. Mech., ASCE*, 130(6), 635-645.
- Guo, P. J. 2000. Modelling granular materials with respect to stress-dilatancy and fabric: A fundamental approach. *Ph.D. Dissertation, Civil Engrg. Dept., University of Calgary*, 375 p.
- Hansen, B. 1958. Lines ruptures regarded as narrow rupture zone, basic equation based on kinematic conditions. *Proceedings of Conference of earth pressure Problems, Brussels, Belgium*, 39-51.
- Li, X.S., and Dafalias, Y.F. 2000. Dilatancy for cohesionless soils. *Geotechnique*, 50(4), 449-460.
- Nakata, Y., Murata, H., Yasufuku, N., Hyodo, M. and Nishikawa, A. 1992. Deformation characteristics of sand subjected to drained cyclic loading. *Technical Report of the Yamaguchi University*, 5(1), 11-21.
- Newland, P. L. and Alley, B. H. 1957. Volume change in drained triaxial tests on granular materials. *Geotechnique*, 7(1), 17-34.
- Oda, M. 1972. Initial fabrics and their relations to mechanical properties of granular material, *Soils and Foundations*, 12(1), 17-36.
- Oda, M. and Koishikawa, I. 1979. Effect of strength anisotropy on bearing capacity of shallow footing in a dense sand. *Soils and Foundations*, 19(3), 15-28.
- Reynolds, O. 1885. On the dilatancy of media composed of rigid particles in contact. *Phil. Mag.*, 5(2), 469-481.
- Rowe, P.W. 1962. The stress-dilatancy relation for static equilibrium of an assembly of particles in contact. *Proc. of the Royal Society of London*, Vol 269, Series A, 500-527.
- Taylor, D. W. 1948. *Fundamentals of soil mechanics*, Wiley, New York.
- Vaid, Y.P. and Saivathayalan, S. 2000. Fundamental factors affecting liquefaction susceptibility of sands. *Canadian Geotechnical Journal*, 37, 592-606.
- Wan, R. and Guo, P.J. 2004. Stress dilatancy and fabric dependencies on sand behavior. *Journal of Engineering Mechanics*, 130(6), 635-645.
- Wan, R. and Guo, P.J. 2001a. Effect of microstructure on undrained behaviour of sands, *Canadian Geotechnical Journal*, 38, 16-28.
- Wan, R., and Guo, P.J. 2001b. Drained cyclic behaviour of sand with fabric dependence. *J. of Eng. Mech., ASCE*, 127(1), 1106-1116.
- Wan, R., & Guo, P.J. 1998. A simple constitutive model for granular soils: Modified stress-dilatancy approach. *Computers and Geotechnics*, 22(2), 109-133.
- Zlatovic, S., and Ishihara, K. 1997. Normalized behaviour of very loose non-plastic soils: effects of fabric. *Soils and Foundations*, 37(4), 47-56.